Published in final edited form as:
Cancer Res. 2008 August 15; 68(16): 6496–6506. doi:10.1158/0008-5472.CAN-07-5756.

AMPK Signaling Results in Cytoplasmic Sequestration of p27

John D. Short[1,*], **Kevin D. Houston**[1,*], **Ruhee Dere**[1], **Sheng-Li Cai**[1], **Jinhee Kim**[1], **Charles L. Johnson**[1], **Russell R. Broaddus**[2], **Jianjun Shen**[1], **Susie Miyamoto**[3], **Fuyuhiko Tamanoi**[3], **David Kwiatkowski**[4], **Gordon B. Mills**[5], and **Cheryl Lyn Walker**[1,6]

[1]Department of Carcinogenesis, University of Texas MD Anderson Cancer Center

[2]Department of Molecular Pathology, University of Texas MD Anderson Cancer Center

[3]Department of Microbiology, Immunology and Molecular Genetics University of California, Los Angeles

[4]Department of Medicine Brigham and Women's Hospital and Harvard Medical School

[5]Department of Systems Biology, University of Texas MD Anderson Cancer Center

Abstract

Tuberin, the *Tsc2* gene product, integrates PI3K/MAPK (mitogenic) and LKB1/AMPK (energy) signaling pathways, and previous independent studies have shown that loss of tuberin is associated with elevated AMPK signaling and altered p27 function. In Tsc2-null tumors and tumor-derived cells from Eker rats, we observed elevated AMPK signaling and concordant cytoplasmic mislocalization of p27. Cytoplasmic localization of p27 in Tsc2-null cells was reversible pharmacologically using inhibitors of the LKB1/AMPK pathway, and localization of p27 to the cytoplasm could be induced directly by activating AMPK physiologically (glucose deprivation) or genetically (constitutively-active AMPK) in Tsc2-proficient cells. Furthermore, AMPK phosphorylated p27 *in vitro* on at least three sites including T170 near the NLS, and T170 was demonstrated to determine p27 localization in response to AMPK signaling. p27 functions in the nucleus to suppress Cdk2 activity, and has been reported to mediate an anti-apoptotic function when localized to the cytoplasm. We found that cells with elevated AMPK signaling and cytoplasmic p27 localization exhibited elevated Cdk2 activity, which could be suppressed by inhibiting AMPK signaling. In addition, cells with elevated AMPK signaling and cytoplasmic p27 localization were resistant to apoptosis, which could be overcome by inhibition of AMPK signaling and relocalization of p27 to the nucleus. These data demonstrate that AMPK signaling determines the subcellular localization of p27, and identifies loss of integration of pathways controlling energy balance, the cell cycle and apoptosis due to aberrant AMPK and p27 function as a feature of cells that have lost the *Tsc2* tumor suppressor gene.

Keywords

AMPK; TSC2; p27

Introduction

Tuberous Sclerosis Complex (TSC) is an autosomal dominant hereditary syndrome leading to the development of hamartomas in several organs including the brain, skin, kidney, heart

[6]To whom correspondence should be addressed: Department of Carcinogenesis UT MD Anderson Cancer Center 1808 Park Road 1C, PO Box 389 Smithville, TX 78957 cwalker@wotan.mdacc.tmc.edu Phone: 512−237−9550 Fax: 512−237−2475.
[*]These authors contributed equally to this work

and lungs (1). Inactivating mutations in either the *TSC1* gene or the *TSC2* gene encoding hamartin and tuberin, respectively cause TSC, and loss of heterozygosity for either *TSC1* or *TSC2* is a common occurrence in hamartomas of patients with TSC (1). At the molecular level, tuberin interacts with hamartin and functions as a GTPase activating protein (GAP) for the small GTPase Rheb (Ras homology enriched in brain) (1,2). This tuberin-mediated decrease in Rheb-GTP levels inactivates mTOR signaling, leading to inactivation of ribosomal protein S6 kinase (S6K) and 4E-BP1, resulting in decreased protein synthesis and cell growth (3).

Tuberin is phosphorylated by AKT in response to PI3K signaling, and this phosphorylation inhibits tuberin-mediated repression of Rheb, activating mTOR signaling to increase protein synthesis (2). In addition, loss of tuberin and the subsequent increase in S6K activity has been reported to lead to an autoregulatory negative feedback loop that inhibits PI3K signaling, since S6K phosphorylates and inhibits insulin receptor substrate 1(IRS1) (4-6). Additionally, loss of Tsc1/Tsc2 impairs AKT signaling through PDGFR and EGFR downregulation (7). Tuberin is also phosphorylated by AMP-activated protein kinase (AMPK), a heterotrimeric protein complex that responds to changes in cellular AMP/ATP ratios to regulate energy consuming (anabolic) and energy generating (catabolic) processes (8,9). Phosphorylation of tuberin by AMPK enhances tuberin repression of mTOR signaling, and tuberin is essential for altered cell growth in response to energy deprivation (9). Thus, tuberin functions in the cell as a rheostat to integrate mitogenic and energy sensing pathways.

In addition to regulating cell growth via mTOR signaling, tuberin is also thought to influence both the protein levels, and subcellular localization of p27 (10). p27 is a member of the Cip/Kip family of cyclin-dependent kinase inhibitors (CKIs) that function to negatively regulate cyclin A- and cyclin E-Cdk2 complexes in the nucleus, preventing cell cycle progression (11). p27 stability and localization are regulated primarily by phosphorylation, which can target p27 for proteosome degradation or promote interaction with 14−3−3 and lead to cytoplasmic retention of this CKI (10). In addition, p27 degradation is mediated by different processes in the cytosol and nucleus, potentially contributing to selective cytoplasmic or nuclear accumulation (12). Cells lacking tuberin have been reported to exhibit reduced p27 expression in some cases, and in others, cytoplasmic mislocalization of p27. Tuberin has also been reported to directly interact with p27 to regulate p27 interaction with 14−3−3 and Skp1/cullin/F-box protein (SCF) complex, an E3 ubiquitin ligase involved in targeting p27 for degradation (13-15). However, an understanding of sometimes discordant findings on p27 expression in Tsc2-null cells as well as a mechanistic basis for modulation of p27 function in these cells has been elusive.

Loss of AKT activity was recently found to activate AMPK via modulation of AMP levels, and AMPK activity is elevated in *Tsc2*$^{-/-}$ MEFs (16). This suggests that elevated AMPK signaling may be a consistent feature of tuberin-null cells due to the aforementioned negative feedback loop that represses AKT in these cells. In addition, AMPK signaling was recently found to phosphorylate p27 and regulate p27 protein levels (17), leading us to hypothesize that AMPK signaling could be responsible for altered p27 localization and activity in tuberin-null cell lines and tumors.

Using a rat model for *Tsc2*-deficiency, we found that tumors and tumor-derived cell lines lacking tuberin had activated AMPK and exhibited cytoplasmic localization of p27. Furthermore, modulation of AMPK signaling was demonstrated to directly control subcellular localization of p27 independent of tuberin expression, due in part to phosphorylation of p27 at T170. In addition, tuberin-null tumors and cell lines with constitutively activated AMPK exhibited increased Cdk2 activity and resistance to apoptosis

that was overcome by inhibition of AMPK signaling and re-localization of p27 to the nucleus.

Materials and Methods

Animal maintenance and tissue culture

p27$^{+/-}$ male mice were provided by Dr. Christopher Kemp and crossed with *Tsc2*$^{+/-}$ mice (18,19). Because of morbidity associated with gastrointestinal blockage and pituitary tumors, animals were sacrificed at 5−6 months of age for analysis of kidney lesions. Mice and Eker rats (*Tsc2*$^{Ek/+}$) (20,21) were maintained in a closed colony at UTMDACC. The ELT-3 cell line (maintained in DF8 media) was previously described (20). All other cell lines (NIH3T3, HEK293, *Tsc2*$^{+/+}$, *Tsc2*$^{-/-}$, *p27*$^{+/+}$ and *p27*$^{-/-}$ MEFs) were maintained in DMEM supplemented with 10% FBS. Both *Tsc2*$^{+/+}$ and *Tsc*$^{-/-}$ MEFs are p53-null as described previously (7).

Plasmid Preparation and Transfection

The FLAG-p27-WT construct was generated by subcloning a PCR product generated from rat p27 cDNA into the pCMV-Tag2-FLAG expression vector (Stratagene). The GST-p27-WT construct was generated by digesting the p27 coding sequence from Flag-p27-WT and ligating into pGEX-6P-1. Mutagenesis was performed using the QuickChange XL site-directed mutagenesis kit (Stratagene). AMPK-α constructs (9) were a gift of Drs. S. Fischer and K. Guan. Transient transfections were performed using Lipofectamine2000 (Invitrogen) and Effectene (Qiagen).

Subcellular fractionation

Subcellular fractionation of cells to yield nuclear and cytosolic fractions was performed as described previously (22). Briefly cells were resuspended in hypotonic buffer and disrupted using a Dounce homoginizer and the crude nuclei pelleted by centrifugation. The supernatant was collected as the cytosolic fraction and the crude nuclei was further purified to yield the nuclear fraction.

Antibodies and Reagents

Tuberin (Epitomics), Cdk2 (Santa Cruz Biotechnology, Inc.), AMPK-α1 and AMPK-α2 (Abcam), p27 (K5020) (BD Transduction Laboratories), Sp1 (Upstate Biotechnology), AMPK-α, phospho-AMPK-α(T172), ACC, phospho-ACC (S79), S6 and phosho-S6 (Cell Signaling Technology). Compound C and H-89 (CalBiochem).

Immunocytochemistry/ Immunohistochemistry

Cells either transfected or treated as indicated were fixed followed by permeabilization. Cells were stained using mouse anti-p27, rabbit anti-HA (Santa Cruz Biotechnology), and mouse anti-Flag (Sigma) antibodies. Secondary antibodies were conjugated with FITC (abcam), (goat anti-mouse or goat anti-rabbit), or Texas Red (Jackson ImmunoResearch Laboratories) (donkey anti-mouse). For endogenous p27 staining, slides were blocked using the Endogenous Avidin/Biotin blocking kit (Zymed) before applying the primary antibody. Primary antibodies were recognized using biotin conjugated donkey anti-mouse (Abcam) and streptavidin conjugated FITC or Texas Red (Molecular Probes). The VectaShield mounted coverslips were visualized by conventional microscopy with a fluorescent attachment (Olympus). MagnaFire version 2.1 C (Olympus) software was used for image acquisition.

For immunohistochemistry, fixed tissues were incubated with an anti-p27 antibody, recognized using a Hrp-conjugated anti-mouse antibody. Slides were stained using DAB and visualized by conventional microscopy.

In vitro Kinase Assays

GST-p27 fusion proteins were induced and purified using BL21-Star cells, followed by cleavage from GST using PreScission Protease (~32-units) (Amersham Pharmacia Biotech). Purified recombinant p27 protein was analyzed by SDS-PAGE and quantitated using a BCA Protein Quantitation kit (Pierce, Rockford, IL). AMPK (10mU; Upstate) was incubated with 1-μg of the indicated recombinant p27 protein for 15-min at 30°C. The reactions were then separated by SDS-PAGE, dried, and visualized.

For Cdk2 kinase assays, lysates were immunoprecipitated overnight at 4°C using 1-μg anti-Cdk2 antibody (Santa Cruz Biotechnology) along with 20-μl of Protein-G/Sephadex. Immunoprecipitates were then washed three times each with Lysis Buffer and Cdk2 kinase buffer (50mM Tris-HCl (pH7.4), 10mM $MgCl_2$, 1mM DTT, 1mM Na_3VO_4, and 1mM NaF). Immunoprecipitates were resuspended in 25-μl Cdk2 kinase buffer and incubated at 30°C with 2.5-μg Histone H1 (Roche), 5-μCi γ-^{32}P-ATP, and 50-μM ATP for 30-min. The reaction was terminated with 20-μl 2X-SDS-SB, separated by PAGE, dried and visualized. All blots were visualized and quantitated using a Typhoon 9415 Variable Mode Imager (Amersham Pharmacia Biotech).

Apoptosis Assays

For TUNEL staining, formalin-fixed paraffin sections were processed and stained using a FragEl DNA fragmentation kit (Calbiochem). Five tumor fields (20X) from kidneys of 5−6 month old *Tsc2*$^{+/-}$/*p27* mice were scored blind as to genotype for TUNEL immunoreactivity by a board-certified pathologist. Total number of tumor-bearing animals scored for each genotype were *Tsc2*$^{+/-}$/*p27*$^{+/+}$ n=3, *Tsc2*$^{+/-}$/*p27*$^{+/-}$ n=6, and *Tsc2*$^{+/-}$/*p27*$^{-/-}$ n=12.

For caspase assays, protein lysates (~40-μg) were added to a 200-μl reaction mixture containing 50-μM Ac-DEVD-AFC (BIOMOL) in 1x Caspase Reaction Buffer (25mM HEPES, 50mM NaCl, 0.05% CHAPS, 5mM DTT, 0.5mM EDTA and 5% glycerol) for 90-min at 37°C. Production of AFC was measured using a FL6000 Microplate Fluorescent Reader (BIO-TEK).

Results

Elevated AMPK signaling correlates with cytoplasmic localization of p27 in *Tsc2*$^{-/-}$ cells and tumors

Eker rats are heterozygous for the *Tsc2* tumor suppressor gene (*Tsc2*$^{Ek/+}$) and develop uterine leiomyoma subsequent to loss of the wild-type Tsc2 allele with a high frequency (23). We examined a uterine tumor-derived cell line, ELT-3 (20) and uterine tumors from Eker rats for localization of p27. Endogenous p27 was detected only in the cytosolic fraction of ELT-3 cells grown in the absence or presence of serum, and immunocytochemistry revealed diffuse cytoplasmic staining without nuclear concentration of p27 in these cells (Figure 1A). Additionally, even when a Flag-tagged wild-type p27 construct (Flag-p27-WT) was overexpressed in ELT-3 cells, the vast majority of exogenous p27 was retained in the cytosolic fraction of these cells (Supplemental Figure 1A). In contrast, in NIH3T3 (*Tsc2*$^{+/+}$) cells, endogenous p27 was detected in both the nuclear and cytosolic fractions and immunocytochemistry showed concentrated nuclear staining of endogenous p27 (Figure 1A). Immunohistochemistry analyses of uterine leiomyomas from Eker rats also revealed an aberrant cellular localization pattern of p27. p27 was detected solely in nuclei of normal

myometrial cells (Figure 1B-left & middle), whereas over half the tumors (13/22) had strong cytoplasmic p27 immunoreactivity accompanied by nuclear staining (Figure 1B-middle) and approximately 20% (5/22) had predominantly cytoplasmic p27 with little or no nuclear reactivity (Figure 1B-right). Fewer than 20% (4/22) were negative for p27 or had predominantly nuclear staining reactivity.

Furthermore, we examined p27 localization in *Tsc2*$^{-/-}$ mouse embryonic fibroblasts (MEFs) and in microscopic kidney lesions of *Tsc2*$^{+/-}$ mice predisposed to develop renal cell carcinoma following spontaneous loss of the wild-type *Tsc2* allele (19). p27 was primarily detected in the cytosolic fraction of *Tsc2*$^{-/-}$ MEFs, whereas p27 was localized to both the cytosolic and nuclear fractions of MEFs derived from *Tsc2*$^{+/+}$ mice (Figure 1C). Moreover, p27 was readily detectable in the cytoplasm of microscopic kidney lesions from compound heterozygous *Tsc2*$^{+/-}$/*p27*$^{+/+}$ or *Tsc2*$^{+/-}$/*p27*$^{+/-}$ mice that retained p27 expression (Figure 1C).

We also evaluated AMPK signaling, which, similar to the observation from Hay's group (16), was elevated in *Tsc2*$^{-/-}$ MEFs as indicated by increased phosphorylation of AMPK-α at T172 (Figure 2A). ELT-3 cells also exhibited characteristic downregulation of AKT due to negative feedback from elevated mTOR signaling (Supplemental Figure 1B), and elevated AMPK signaling as indicated by both AMPK-α phosphorylation and increased phosphorylation of ACC at S79, a direct target of AMPK (Figure 2A). Since ELT-3 cells exhibited increased AMPK signaling and cytoplasmic localization of p27, we examined primary uterine leiomyomas from Eker rats for activation of the AMPK signaling pathway. Similar to ELT-3 cells, uterine leiomyomas from Eker rats exhibited elevated phospho-S6 levels characteristic of elevated mTOR signaling associated with loss of tuberin function in these tumors (Figure 2B,Supplemental Figure 1B) (23). Both AMPK-α1 and AMPK-α2 could be detected in uterine leiomyomas and normal myometrium of Eker rats, with similar p27 protein levels (Figure 2B). However, uterine leiomyomas from Eker rats exhibited increased levels of phosphorylated AMPK-α at T172 as well as a slower migrating form of phosphorylated AMPK-α and total AMPK-α compared with normal myometrium from Eker rats (Figure 2B). These data led us to explore a possible linkage between AMPK signaling and altered p27 localization.

AMPK signaling regulates cytoplasmic localization of p27

To investigate whether AMPK signaling could alter the subcellular localization of p27, we modulated AMPK activity in both tuberin-deficient and tuberin-proficient cells to determine the impact of AMPK on p27 localization. Initially, ELT-3 cells (with constitutively active AMPK and cytoplasmic p27) were treated with pharmacological inhibitors of the LKB1/AMPK signaling pathway, H-89 and Compound C, and p27 localization was observed by immunocytochemistry. H-89 has been reported to inhibit PKA-mediated phosphorylation of LKB1 (24) and to counteract certain cellular effects of AMPK activators (25), while Compound C is a direct AMPK inhibitor (26). As shown in Figure 3A, the percentage of cells with nuclear p27 staining increased while the percentage of cells with cytoplasmic p27 staining decreased following a 5-hour treatment with either H-89 or Compound C. Additionally, subcellular fractionation confirmed nuclear relocalization of p27 in ELT-3 cells following a 3-hour treatment with H-89 (data not shown).

AMPK activity was also modulated in tuberin-proficient NIH3T3 cells by glucose deprivation, which activates AMPK. Glucose deprivation of NIH3T3 cells in the presence or absence of serum caused an increase in AMPK signaling as determined by increased phosphorylation of AMPK-α (T172) and ACC (S79) (Figure 3B). Additionally, glucose deprivation led to cytosolic retention of p27, and diffuse cytoplasmic staining without nuclear retention of p27 as revealed by both subcellular fractionation and

immunocytochemistry (Figure 3B). Furthermore, the PI3K and MEK/MAPK inhibitors, LY294002 and PD98059, had no effect on p27 localization or phospho-AMPK-α levels while blocking their respective targets in glucose-deprived NIH3T3 cells (Supplemental Figure 2).

Finally, Flag-p27-WT was transiently co-expressed with HA-tagged wild-type AMPK-α1 (WT-AMPK-α1), constitutively active AMPK-α1 (CA-AMPK-α1) or dominant negative AMPK-α1 (DN-AMPK-α1) in NIH3T3 cells to further determine whether AMPK signaling altered p27 localization. Exogenous Flag-p27-WT exhibited concentrated nuclear staining in approximately 40% of cells when overexpressed alone or 30% of cells that co-expressed WT-AMPK-α1 (Figure 3C). However, < 10% of cells overexpressing CA-AMPK-α1 showed concentrated nuclear staining of Flag-p27-WT while cells that expressed DN-AMPK-α1 showed concentrated nuclear staining of Flag-p27-WT in over 70% cells (Figure 3C). Taken together, these data indicate that AMPK signaling regulates localization of p27 both in the presence or absence of growth factors and that regulation of p27 localization is AMPK dependent in both tuberin-proficient and tuberin-deficient cells.

T170 mediates cytoplasmic localization of p27 in response to AMPK signaling

Using AMPK target recognition consensus sequences, we identified three potential AMPK recognition sequences in p27 that are highly conserved across multiple species: S83, T170 and T197 (Figure 4A). Of these, the human terminal threonine (T198) has been previously demonstrated to be phosphorylated by AMPK (17). We performed *in vitro* kinase assays to determine whether AMPK could phosphorylate murine p27 at one or more of these residues. AMPK phosphorylated recombinant murine wild-type p27 (p27-WT) *in vitro*, and exhibited a 5-fold increase in phosphorylation in the presence of AMP (Figure 4B). A 20−35% reduction in p27 phosphorylation was observed when S/T was mutated to alanine at S83, T170 or T197 compared to p27-WT, and all three mutations in combination led to a >50% reduction in p27 phosphorylation (Figure 4B). These data suggest that AMPK can directly phosphorylate p27 directly at T170, the carboxy terminal threonine residue (hT197/mT198), and potentially other sites such as S83 as well.

We next investigated whether mutations of these potential AMPK target sites could alter localization of p27. Alanine substitution of T170 (Flag-p27-T170A) or mutation to a phosphomimetic residue (Flag-p27-T170D) significantly changed p27 localization, from 40% nuclear p27 in Flag-p27-WT expressing cells to >50% and approximately 20% in case of Flag-p27-T170A and Flag-p27-T170D, respectively (Figure 4C). Mutation of S83 (Flag-p27-S83A) or T197 (Flag-p27-T197A) to alanine did not alter localization of p27 (Figure 4C). Additionally, Flag-p27-T170A exhibited concentrated nuclear staining (~40% cells) when co-expressed with CA-AMPK-α1. In contrast, nuclear Flag-p27-WT, Flag-p27-S83A or Flag-p27-T197A staining was significantly lower than Flag-p27-T170A (<20%) in the presence of CA-AMPK-α1 (Figure 4D). These data indicate that T170 is a primary determinant of p27 localization when AMPK signaling is active, and contributes to retention of p27 in the cytoplasm.

Tuberin-null cells have elevated Cdk2 activity that is reduced by inhibition of AMPK signaling

To identify a possible functional consequence of cytoplasmic localization of p27 in tuberin-null cells, we examined Cdk2 activity in both $Tsc2^{+/+}$ cells and $Tsc2^{-/-}$ cells under conditions in which growth and Cdk2 activity are normally repressed. Cdk2 activity from $Tsc2^{-/-}$ MEFs was 4-fold higher than Cdk2 activity of $Tsc2^{+/+}$ MEFs when cells were at 100% confluency, and more than 40-fold greater when cells were deprived of serum (Figure 5A).

Since Cdk2 kinase activity was high in ELT-3 cells with activated AMPK and cytosolic p27 (Figure 5B), we sought to determine whether inhibition of AMPK signaling (and relocalization of p27 to the nucleus) would inhibit Cdk2 kinase activity. ELT-3 cells treated with Compound C for 5-hours or 24-hours, which relocalized p27 to the nucleus (Figure 3A) and inhibited AMPK activity, exhibited lower Cdk2 kinase activity than non-treated cells (Figure 5B). These data suggest that exclusion of p27 from the nucleus is associated with elevated Cdk2 kinase activity, which can be reduced by relocalization to the nucleus. Additionally, as shown in Figure 5C, Flag-p27-T170A (which is retained in the nucleus) (Figure 4D) was more efficient at inhibiting Cdk2 kinase activity in ELT-3 cells compared to Flag-p27-WT, which is mislocalized to the cytoplasm in these cells. Thus, cytoplasmic sequestration of p27 inhibits the ability of this CKI to repress Cdk2 activity.

p27 localization mediates an antiapoptotic function of AMPK

Another possible functional consequence of cytoplasmic localization of p27 due to elevated AMPK signaling is resistance to apoptosis, and we have recently shown that p27 mediates a decision to undergo apoptosis or autophagy in tumor cells (17). Defects in AMPK activation have been previously linked to increased sensitivity to cell death (27), and cytosolic p27 has been reported to inhibit apoptosis upon serum deprivation (28). To investigate a potential linkage between AMPK signaling, cytoplasmic p27 and apoptosis, NIH3T3 cells and $Tsc2^{+/+}$ MEFs (with low levels of activated AMPK and nuclear p27) or tuberin-null ELT-3 cells and $Tsc2^{-/-}$ MEFs (with high levels of activated AMPK and cytoplasmic p27) were deprived of serum and apoptosis measured both before and after serum starvation by quantifying the percentage of nuclei exhibiting bright DAPI staining or nuclear fragmentation. As shown in Figure 6A, both NIH3T3 cells and $Tsc2^{+/+}$ MEFs exhibited an increase in the percentage of nuclei with apoptotic features 24-hours after removal of serum. While both $Tsc2^{-/-}$ MEFs and ELT-3 cells had a high background level of apoptotic nuclei when grown in serum, removal of serum failed to increase the percentage of nuclei with apoptotic features in tuberin-null ELT-3 cells or $Tsc2^{-/-}$ MEFs (Figure 6A). Apoptosis was also quantified by measuring Caspase-3/Caspase-7 activity following 5-, 10-, and 20-hours of serum starvation. Both NIH3T3 cells and $Tsc2^{+/+}$ MEFs exhibited >15-fold increase in caspase activity as early as five hours after serum removal that was sustained throughout the 20-hour time-course (Figure 6B). ELT-3 cells and $Tsc2^{-/-}$ MEFs with cytoplasmic p27 exhibited dramatically lower caspase activity than NIH3T3 cells and $Tsc2^{+/+}$ MEFs with primarily nuclear localized p27 at all time points of serum withdrawal, although $Tsc2^{-/-}$ MEFs and ELT-3 cells did eventually exhibit a slight increase in caspase activity after 20-hours of serum withdrawal (Figure 6B). Similarly, in $p27^{-/-}$ MEFs and $p27^{+/+}$ MEFs, the absence of p27 correlated with increased sensitivity to apoptosis. Serum-starvation for 24-hours led to a >13-fold increase in caspase activity in $p27^{-/-}$ MEFs that express a truncated p27 protein lacking the N-terminal nuclear export signal (29) resulting in its nuclear retention (data not shown), while $p27^{+/+}$ MEFs were refractory to the induction of apoptosis (Figure 6B), which correlated with high levels of cytosolic p27 in these cells (data not shown). These correlative data demonstrated that cells with activated AMPK and cytoplasmic p27 are resistant to the induction of apoptosis by serum deprivation.

To determine whether there was a direct link between AMPK activation, cytoplasmic localization of p27, and resistance to apoptosis, NIH3T3 cells were deprived of glucose prior to serum-starvation. Glucose deprivation (which activates AMPK and sequesters p27 in the cytoplasm, Figure 3B), markedly delayed caspase activation induced by serum-starvation up to 20 hours in these cells (Figure 6B). In addition, ELT-3 cells and $Tsc2^{-/-}$ MEFs were treated with Compound C to determine whether inhibition of AMPK signaling and altered localization of p27 (Figures 3A and 6C) could alter susceptibility to apoptosis in these cells. Treatment with Compound C led to an increase in caspase activation after 5 (Figure 6C) or

20 (data not shown) hours of serum deprivation. These data indicate that modulation of AMPK signaling and p27 localization alters susceptibility to apoptosis, whereas inhibition of AMPK activity induces an apoptosis-sensitive phenotype that is correlated with a loss of cytoplasmic p27.

To investigate a potential linkage between p27 and resistance to apoptosis in tuberin-null tumors, *Tsc2*$^{+/-}$ mice predisposed to renal tumorigenesis (19,30) were crossed with *p27*$^{+/-}$ mice, which develop tumors at sites other than the kidney with a short latency (18). *Tsc2*$^{+/-}$/*p27*$^{+/+}$, *Tsc2*$^{+/-}$/*p27*$^{+/-}$ and *Tsc2*$^{+/-}$/*p27*$^{-/-}$ mice developed multiple, bilateral renal cell carcinomas, although neither tumor incidence nor multiplicity (Supplemental Table 1) was different in p27-proficient (*p27*$^{+/+}$) versus p27-deficient (*p27*$^{+/-}$ or *p27*$^{-/-}$) animals, which was interesting given that p27 deficiency predisposes to tumors at several other organ sites. However, the apoptotic index was significantly higher in tumors that developed in p27-deficient animals (*Tsc2*$^{+/-}$/*p27*$^{-/-}$ and *Tsc2*$^{+/-}$/*p27*$^{+/-}$ mice) relative to tumors that developed in p27-proficient animals (*Tsc2*$^{+/-}$/*p27*$^{+/+}$ mice) (Figure 6D). This finding was consistent with the antiapoptotic activity of p27 observed in Tsc2-null cells *in vitro* (Figure 6A, B and C), and may underlie the observation that p27-deficiency did not significantly increase renal tumor development in *Tsc2*$^{+/-}$ mice.

Discussion

We found that tuberin-null cell lines and tumors exhibit activated AMPK signaling and cytoplasmic localization of p27. Furthermore, we demonstrated that activation of AMPK signaling causes cytoplasmic localization of p27 in both tuberin-proficient and tuberin-deficient cells, and that T170 of p27 can be phosphorylated by AMPK *in vitro*, and regulates p27 localization in response to AMPK signaling. We also found that cells with activated AMPK and cytoplasmic p27 had elevated Cdk2 activity that could be inhibited by inactivating AMPK and relocalizing p27 to the nucleus. Lastly, we found elevated AMPK signaling and cytoplasmic p27 promoted resistance to apoptosis, which could be reversed by inhibition of AMPK signaling and decreasing levels of cytoplasmic p27.

We have shown that tuberin-null cells and tumors from Eker rats have elevated AMPK signaling, confirming a previous report showing that AMPK signaling is elevated in *Tsc2*−/− MEFs (16). One possible mechanism for activated AMPK signaling in tuberin-null cells is decreased IRS1 and AKT activity, due to the negative feedback from S6K to IRS1 in tuberin-null cells [supplemental data and (4-6)], since AKT signaling reportedly antagonizes AMPK activity (16,31). Alternatively, the elevation of reactive oxygen species associated with loss of either *Tsc1* or *Tsc2* (32,33) in cells and tumors could also contribute to elevated AMPK signaling, since AMPK has been shown to be redox sensitive (34).

Previous studies have linked tuberin with p27 stabilization and localization (13,15,35). p27 was reported to be more unstable in tuberin-null cells and mislocalized to the cytosol, and overexpression of *Tsc2* was reported to increase p27 protein levels (15,35). In addition, tuberin was reported to interact with p27 and increase nuclear p27 by regulating the interaction between AKT-phosphorylated p27 and 14−3−3 (13). However, tuberin-null cell lines and tumors exhibit decreased IRS1 and AKT activity due to the aforementioned negative feedback from S6K to IRS1 [data not shown and (4-6)]. Therefore, an AKT-dependent mechanism as proposed by Rosner *et al*. (13) is unlikely to be responsible for mislocalization of p27 in tuberin-null cells and tumors. Our study provides an alternative mechanism in which the relationship between *Tsc2* and p27 and subcellular localization of this CKI can be understood in the context of activated AMPK signaling.

Localization of p27 is a complex process that is affected by phosphorylation at multiple residues (36). For example, phosphorylation of p27 at S10 by hKIS leads to it's cytoplasmic localization and degradation, whereas phosphorylation at S10 by the Mirk/dyrk1B kinase does not alter p27 localization (36). Additionally, phosphorylation of human p27 at T157/T198 by AKT or phosphorylation at T198 by RSK also alters subcellular localization of p27 through stabilization and interaction with 14−3−3 proteins (10,36). S10 of p27 is not a potential AMPK target site, and T157 of p27 is not a conserved amino acid residue in rodents. Moreover, modulation of AKT or RSK signaling had no affect on p27 localization (supplemental data), and similar to our data, mutation of T198 had no impact on p27 localization in a report showing that AMPK phosphorylates this residue on p27 (17). Instead, we found that T170, a conserved putative AMPK target site near the p27 NLS was a primary determinant of murine p27 localization in response to AMPK signaling and this site was phosphorylated by AMPK *in vitro*. This is the first report to identify T170 as a site regulating localization of p27, although it is not clear at this time if AMPK directly phosphorylates p27 at T170 *in vivo*.

Cytosolic localization of p27 sequesters p27 from Cdk proteins in the nucleus. Previous reports have shown that Cdk2 activity is elevated in $Tsc2^{-/-}$ EEF8 cells, and this activity can be inhibited by addition of recombinant p27 (15). We found that Cdk2 activity was elevated in $Tsc2^{-/-}$ MEFs and tuberin-null ELT-3 cells, and that inhibition of AMPK signaling decreased Cdk2 activity in tuberin-null cells. Moreover, we confirmed that p27 localization regulated Cdk2 kinase activity. These data suggest that elevated Cdk2 activity may be a consistent feature of tuberin-null tumors in context of TSC, warranting additional analysis in TSC-associated tumors, with the goal of potentially targeting Cdk2 therapeutically.

In addition, a recent report indicates that cytoplasmic p27 can prevent apoptosis and promote tumorigenicity (28). In fact, transgenic mice expressing p27 that cannot inhibit Cdk2 develop tumors in multiple tissues, and p27 is localized to the cytoplasm in lung tumors from these mice (37). These data are consistent with our observations that kidney lesions that developed in $Tsc2^{+/-}/p27^{+/+}$ mice had lower apoptotic indices than lesions that developed in $Tsc2^{+/-}/p27^{+/-}$ or $Tsc2^{+/-}/p27^{-/-}$ mice. We observed that resistance to apoptosis in response to serum deprivation correlated with activated AMPK signaling and cytoplasmic localization of p27, and that resistance to apoptosis upon serum-starvation in tuberin-null cell lines could be overcome by inhibition of AMPK signaling and reduction in cytoplasmic p27. $Tsc2^{-/-}$ MEFs were previously shown to undergo apoptosis upon serum starvation as measured by caspase cleavage in both $Tsc2^{-/-}$ and $Tsc2^{+/+}$ MEFs, although the relative amount of apoptosis occurring in these cells was not quantitated (6). Our data indicates that although caspase activity is increased upon serum deprivation of both $Tsc2^{+/+}$ and $Tsc2^{-/-}$ cells, the relative caspase activity is much higher in $Tsc2^{+/+}$ cells. Interestingly, Inoki *et al.* have previously examined apoptosis in response to energy depletion. In these studies, *Tsc2*-deficient cells (LEF and EEF8 cell lines) were sensitive to induction of apoptosis in response to 2-deoxyglucose (38), as were $Tsc1^{-/-}$ MEFs. However, EEF8 cells have been previously characterized as having diminished p27 levels (15), and the response of $Tsc2^{-/-}$ MEFs to energy depletion was not examined in their study. Thus, it appears that the relationship of AMPK activity, p27 localization and resistance to apoptosis in *Tsc1/Tsc2*-null cells is likely complex, and will be impacted by both the cell background and apoptotic stimuli used.

Importantly, many targeted therapies, such as receptor tyrosine kinase inhibitors and anti-angiogenic agents, could activate AMPK in tumors via induction of hypoxia and/or nutrient deprivation. In tumors that express p27, altered localization of p27 and repression of apoptosis is a potential adverse effect that could occur as a result of therapy-induced AMPK

activation. Therefore, further studies of the relationship between p27 localization, AMPK signaling and resistance to apoptosis in tumors will allow us to better understand how p27 localization may modulate response to therapy and gain greater insight into the duality of p27 as a regulator of both the cell cycle and cell death.

Supplementary Material

Refer to Web version on PubMed Central for supplementary material.

Acknowledgments

We thank Drs. C. Kemp for the $p27^{+/-}$ mice; Drs. S. Fischer and K. Guan for providing AMPK-α constructs; Drs. D. Chandra and D. Tang for advice regarding the DEVD Caspase assay; and T. Berry, K. Claypool, A. Espejo, and S. Hensley for technical assistance. This work was supported in part by grants as follows: NIEHS (ES07784), NIH (CA41996 and CA32737) to FT; NIH (CA64602 and CA099031) and DAMD (17-02-01-0694) to GBM; and NCI (CA63613), NIEHS (ES08263) and NICHD (HD046282) to CLW.

References

1. Gomez, MR.; Sampson, JR.; Whittemore, VH., editors. Tuberous Sclerosis Complex. 3rd ed. Oxford University Press; Oxford: 1999.
2. Kwiatkowski DJ, Manning BD. Tuberous sclerosis: a GAP at the crossroads of multiple signaling pathways. Hum Mol Genet 2005;14(Spec No. 2):R251–8. [PubMed: 16244323]
3. Crino PB, Nathanson KL, Henske EP. The tuberous sclerosis complex. N Engl J Med 2006;355:1345–56. [PubMed: 17005952]
4. Harrington LS, Findlay GM, Gray A, et al. The TSC1−2 tumor suppressor controls insulin-PI3K signaling via regulation of IRS proteins. J Cell Biol 2004;166:213–23. [PubMed: 15249583]
5. Manning BD, Logsdon MN, Lipovsky AI, Abbott D, Kwiatkowski DJ, Cantley LC. Feedback inhibition of Akt signaling limits the growth of tumors lacking Tsc2. Genes Dev 2005;19:1773–8. [PubMed: 16027169]
6. Shah OJ, Wang Z, Hunter T. Inappropriate activation of the TSC/Rheb/mTOR/S6K cassette induces IRS1/2 depletion, insulin resistance, and cell survival deficiencies. Curr Biol 2004;14:1650–6. [PubMed: 15380067]
7. Zhang H, Cicchetti G, Onda H, et al. Loss of Tsc1/Tsc2 activates mTOR and disrupts PI3K-Akt signaling through downregulation of PDGFR. J Clin Invest 2003;112:1223–33. [PubMed: 14561707]
8. Carling D. The AMP-activated protein kinase cascade--a unifying system for energy control. Trends Biochem Sci 2004;29:18–24. [PubMed: 14729328]
9. Inoki K, Zhu T, Guan KL. TSC2 mediates cellular energy response to control cell growth and survival. Cell 2003;115:577–90. [PubMed: 14651849]
10. Rosner M, Freilinger A, Hengstschlager M. The tuberous sclerosis genes and regulation of the cyclin-dependent kinase inhibitor p27. Mutat Res 2006;613:10–6. [PubMed: 16713332]
11. Slingerland J, Pagano M. Regulation of the cdk inhibitor p27 and its deregulation in cancer. J Cell Physiol 2000;183:10–7. [PubMed: 10699961]
12. Hengst L. A second RING to destroy p27(Kip1). Nat Cell Biol 2004;6:1153–5. [PubMed: 15573093]
13. Rosner M, Freilinger A, Hanneder M, et al. p27Kip1 localization depends on the tumor suppressor protein tuberin. Hum Mol Genet 2007;16:1541–56. [PubMed: 17470459]
14. Rosner M, Hengstschlager M. Tuberin binds p27 and negatively regulates its interaction with the SCF component Skp2. J Biol Chem 2004;279:48707–15. [PubMed: 15355997]
15. Soucek T, Yeung RS, Hengstschlager M. Inactivation of the cyclin-dependent kinase inhibitor p27 upon loss of the tuberous sclerosis complex gene-2. Proc Natl Acad Sci U S A 1998;95:15653–8. [PubMed: 9861025]

16. Hahn-Windgassen A, Nogueira V, Chen CC, Skeen JE, Sonenberg N, Hay N. Akt activates the mammalian target of rapamycin by regulating cellular ATP level and AMPK activity. J Biol Chem 2005;280:32081–9. [PubMed: 16027121]

17. Liang J, Shao SH, Xu ZX, et al. The energy sensing LKB1-AMPK pathway regulates p27(kip1) phosphorylation mediating the decision to enter autophagy or apoptosis. Nat Cell Biol 2007;9:218–24. [PubMed: 17237771]

18. Fero ML, Randel E, Gurley KE, Roberts JM, Kemp CJ. The murine gene p27Kip1 is haplo-insufficient for tumour suppression. Nature 1998;396:177–80. [PubMed: 9823898]

19. Onda H, Lueck A, Marks PW, Warren HB, Kwiatkowski DJ. Tsc2(+/−) mice develop tumors in multiple sites that express gelsolin and are influenced by genetic background. J Clin Invest 1999;104:687–95. [PubMed: 10491404]

20. Howe SR, Gottardis MM, Everitt JI, Goldsworthy TL, Wolf DC, Walker C. Rodent model of reproductive tract leiomyomata. Establishment and characterization of tumor-derived cell lines. Am J Pathol 1995;146:1568–79. [PubMed: 7539981]

21. Walker C, Goldsworthy TL, Wolf DC, Everitt J. Predisposition to renal cell carcinoma due to alteration of a cancer susceptibility gene. Science 1992;255:1693–5. [PubMed: 1553556]

22. Cai SL, Tee AR, Short JD, et al. Activity of TSC2 is inhibited by AKT-mediated phosphorylation and membrane partitioning. J Cell Biol 2006;173:279–89. [PubMed: 16636147]

23. Walker CL, Hunter D, Everitt JI. Uterine leiomyoma in the Eker rat: a unique model for important diseases of women. Genes Chromosomes Cancer 2003;38:349–56. [PubMed: 14566855]

24. Sapkota GP, Kieloch A, Lizcano JM, et al. Phosphorylation of the protein kinase mutated in Peutz-Jeghers cancer syndrome, LKB1/STK11, at Ser431 by p90(RSK) and cAMP-dependent protein kinase, but not its farnesylation at Cys(433), is essential for LKB1 to suppress cell vrowth. J Biol Chem 2001;276:19469–82. [PubMed: 11297520]

25. Ouedraogo R, Wu X, Xu SQ, et al. Adiponectin suppression of high-glucose-induced reactive oxygen species in vascular endothelial cells: evidence for involvement of a cAMP signaling pathway. Diabetes 2006;55:1840–6. [PubMed: 16731851]

26. Zhou G, Myers R, Li Y, et al. Role of AMP-activated protein kinase in mechanism of metformin action. J Clin Invest 2001;108:1167–74. [PubMed: 11602624]

27. Shaw RJ, Bardeesy N, Manning BD, et al. The LKB1 tumor suppressor negatively regulates mTOR signaling. Cancer Cell 2004;6:91–9. [PubMed: 15261145]

28. Wu FY, Wang SE, Sanders ME, et al. Reduction of cytosolic p27(Kip1) inhibits cancer cell motility, survival, and tumorigenicity. Cancer Res 2006;66:2162–72. [PubMed: 16489017]

29. Kiyokawa H, Kineman RD, Manova-Todorova KO, et al. Enhanced growth of mice lacking the cyclin-dependent kinase inhibitor function of p27(Kip1). Cell 1996;85:721–32. [PubMed: 8646780]

30. Kobayashi T, Minowa O, Kuno J, Mitani H, Hino O, Noda T. Renal carcinogenesis, hepatic hemangiomatosis, and embryonic lethality caused by a germ-line Tsc2 mutation in mice. Cancer Res 1999;59:1206–11. [PubMed: 10096549]

31. Kovacic S, Soltys CL, Barr AJ, Shiojima I, Walsh K, Dyck JR. Akt activity negatively regulates phosphorylation of AMP-activated protein kinase in the heart. J Biol Chem 2003;278:39422–7. [PubMed: 12890675]

32. Finlay GA, Thannickal VJ, Fanburg BL, Kwiatkowski DJ. Platelet-derived growth factor-induced p42/44 mitogen-activated protein kinase activation and cellular growth is mediated by reactive oxygen species in the absence of TSC2/tuberin. Cancer Res 2005;65:10881–90. [PubMed: 16322235]

33. Govindarajan B, Brat DJ, Csete M, et al. Transgenic expression of dominant negative tuberin through a strong constitutive promoter results in a tissue-specific tuberous sclerosis phenotype in the skin and brain. J Biol Chem 2005;280:5870–4. [PubMed: 15576369]

34. Choi SL, Kim SJ, Lee KT, et al. The regulation of AMP-activated protein kinase by H(2)O(2). Biochem Biophys Res Commun 2001;287:92–7. [PubMed: 11549258]

35. Soucek T, Rosner M, Miloloza A, et al. Tuberous sclerosis causing mutants of the TSC2 gene product affect proliferation and p27 expression. Oncogene 2001;20:4904–9. [PubMed: 11521203]

36. Borriello A, Cucciolla V, Oliva A, Zappia V, Della Ragione F. p27Kip1 metabolism: a fascinating labyrinth. Cell Cycle 2007;6:1053–61. [PubMed: 17426451]

37. Besson A, Hwang HC, Cicero S, et al. Discovery of an oncogenic activity in p27Kip1 that causes stem cell expansion and a multiple tumor phenotype. Genes Dev 2007;21:1731–46. [PubMed: 17626791]

38. Inoki K, Li Y, Xu T, Guan KL. Rheb GTPase is a direct target of TSC2 GAP activity and regulates mTOR signaling. Genes Dev 2003;17:1829–34. [PubMed: 12869586]

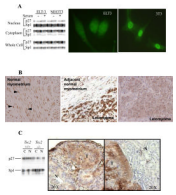

Figure 1.

Cytoplasmic localization of p27 in tuberin-null cell lines and tumors. **(A)** (*left*) Whole-cell, cytosolic, and nuclear lysates generated from the tuberin-null ELT-3 cell line and NIH3T3 cells were immunoblotted using anti-p27 and anti-Sp1 antibodies. (*right*) ELT-3 and NIH3T3 cells were also examined by immunocytochemistry using an anti-p27 antibody (40x original magnification). **(B)** Fixed normal myometrium and leiomyoma tissue from *Tsc2*$^{Ek/+}$ rats were analyzed by immunohistochemistry using an anti-p27 antibody. Representative images (20X magnification for the right image and 40X magnification for the middle and left image) are shown. Arrowheads indicate nuclear p27 immunoreactivity in normal myometrium. **(C)** Cytosolic (C) and nuclear (N) lysates generated from *Tsc2*$^{+/+}$ and *Tsc2*$^{-/-}$ MEFs were analyzed by immunoblotting using anti-p27 and anti-Sp1 antibodies. Sp1 was analyzed as a control for fractionation (*left*). Kidney tissues from *Tsc2*$^{+/-}$ mice containing both normal (N) and tumor (T) tissues were analyzed by immunohistochemistry using an anti-p27 antibody. Representative images (20X magnification) are shown (*right*).

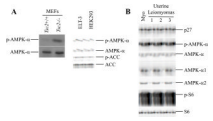

Figure 2.

Elevated AMPK signaling in cell lines and tumors lacking tuberin. **(A)** (*left*) Whole-cell lysates from *Tsc2*$^{+/+}$ and *Tsc2*$^{-/-}$ MEF cells were immunoblotted using an antibody that recognizes phosphorylated AMPK-α at T172 (p-AMPK-α) and an anti-AMPK-α antibody. AMPK-α levels were analyzed as a control for equal loading. (*right*) Whole-cell lysates from ELT-3 cells and HEK293 cells were immunoblotted using anti-p-AMPK-α (T172), anti-AMPK-α, anti-p-ACC (S79) and anti-ACC antibodies. Both AMPK-α levels and ACC levels were analyzed as controls for equal loading. **(B)** Protein lysates from normal uterine tissue (myometrium) and three independent uterine tumors from Eker rats (*Tsc2*$^{Ek/+}$) were normalized and immunoblotted using anti-tuberin, anti-p27, anti-p-AMPK-α (T172), anti-AMPK-α, anti-AMPK-α1, anti-AMPK-α2, anti-p-S6 and anti-S6 antibodies.

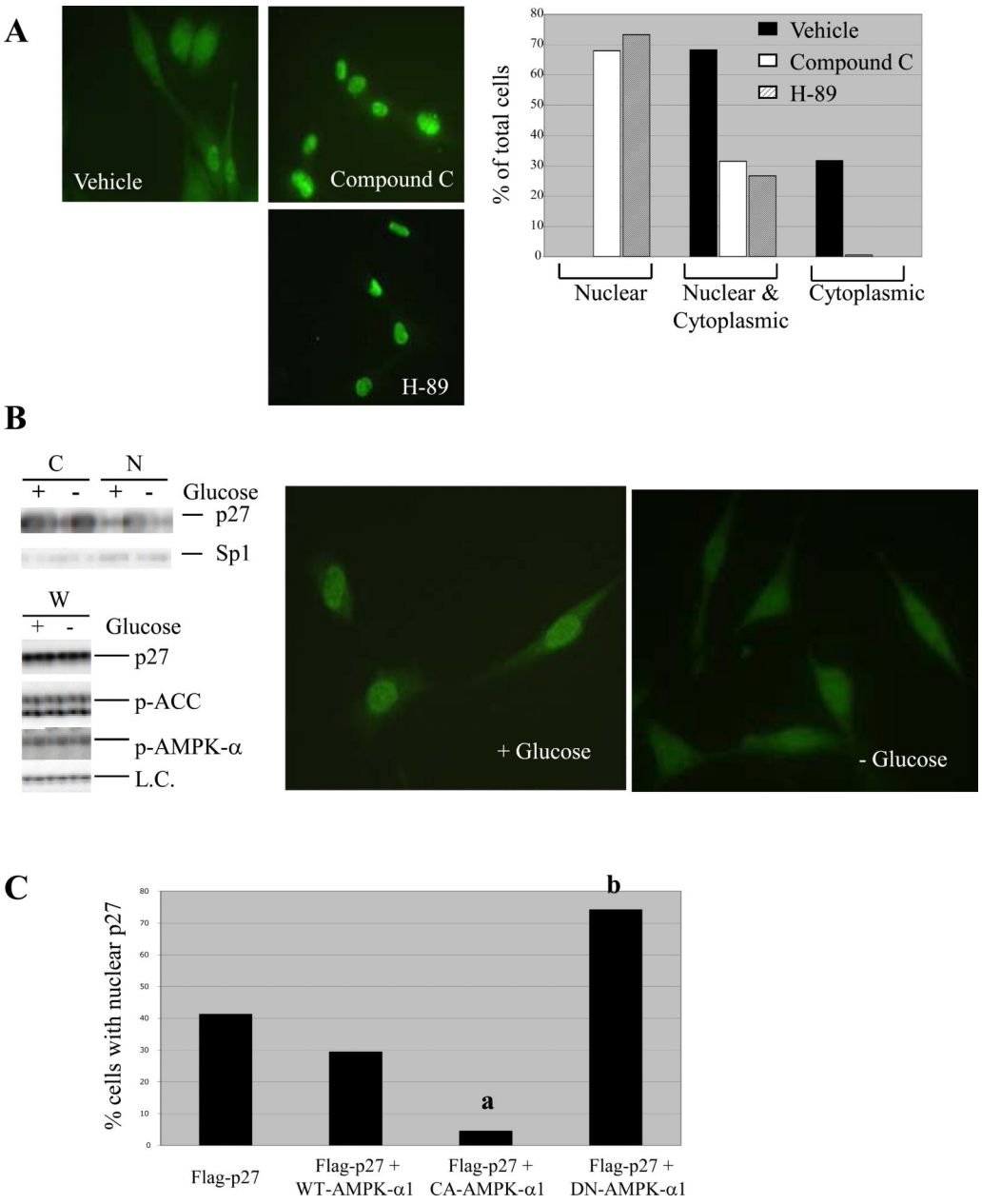

Figure 3.

AMPK signaling regulates subcellular localization of p27. **(A)** (*left*) Tuberin-null ELT-3 cells were treated for 5 hours with 100-nM H-89 or 20-μM Compound C and then visualized by immunocytochemistry using an anti-p27 antibody. Representative images (40X original magnification) are shown, and detection of p27 in the nucleus, cytoplasm, or both compartments was scored as a percentage of total cells analyzed. **(B)** Tuberin-expressing NIH3T3 cells were grown in media without serum in the presence or absence of glucose. Cells were then used to generate whole-cell (W), cytosolic (C) and nuclear (N) lysates. (*top left*) Cytosolic and nuclear lysates were immunoblotted using anti-p27 and anti-Sp1 antibodies. (*bottom left*) Whole-cell lysates were analyzed by immunoblotting using anti-p27, anti-p-AMPK-α (T172) and anti-p-ACC (S79) antibodies. Both p27 levels and levels of a non-specific band (L.C.) indicate equal loading. (*right*) NIH3T3 cells grown in the

presence or absence of glucose were also analyzed by immunocytochemistry using an anti-p27 antibody. Representative images are shown (40x original magnification). **(C)** Tuberin-expressing NIH3T3 cells were transfected with Flag-p27-WT alone or in combination with HA-tagged WT-AMPK-α1, CA-AMPK-α1, or DN-AMPK-α1. Cells were then analyzed by immunocytochemistry using anti-Flag and anti-HA antibodies, and the percentage of cells expressing HA in which exogenous p27 was detected solely in the nucleus was determined. Statistical analysis (Fischer test) showed a significant decrease in the percentage of cells with nuclear Flag-p27-WT when CA-AMPK-α1 was overexpressed (**a**, $p < 0.0001$) and a significant increase in the percentage of cells with nuclear Flag-p27-WT when DN-AMPK-α1 was overexpressed (**b**, $p < 0.0001$).

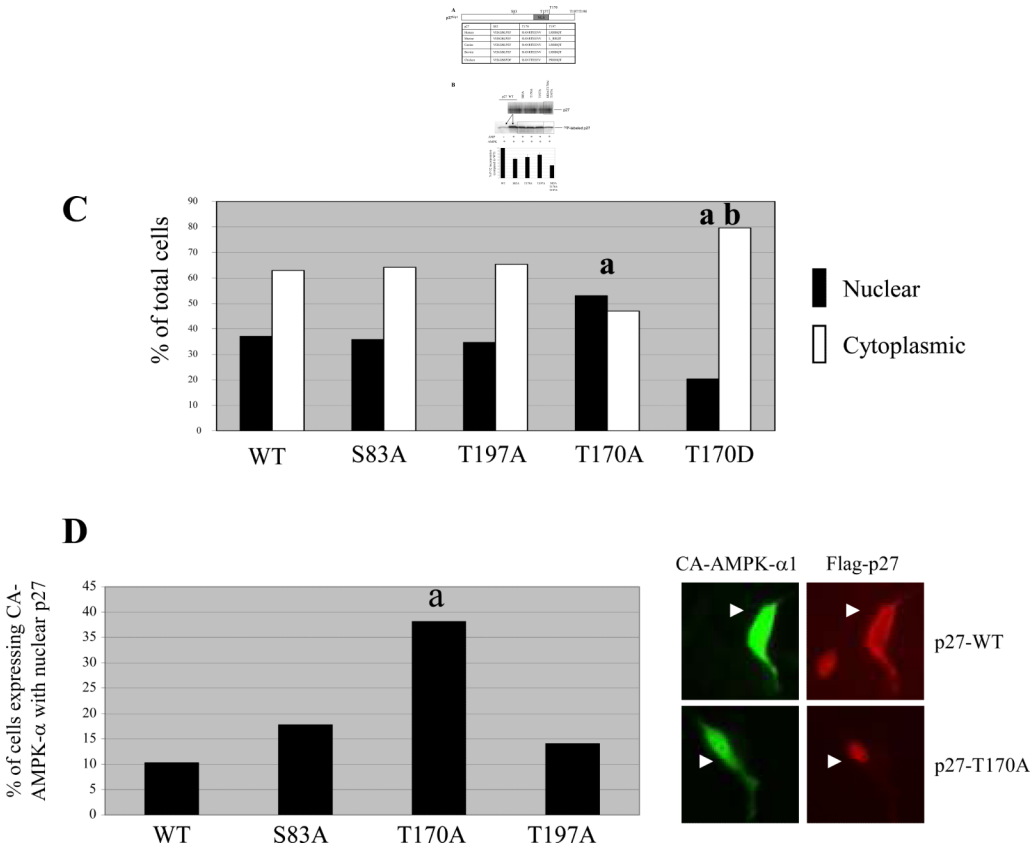

Figure 4.

T170 is a primary determinant of p27 localization in response to AMPK signaling. **(A)** Schematic of p27 showing conservation of amino acid residues at S83, T170 and T197. A table with potential AMPK phosphorylation sites and surrounding amino acid sequences from several species is shown below. **(B)** *In vitro* kinase assays were performed with AMPK utilizing equal amounts of wild-type p27 in the absence or presence of AMP or p27 mutated at potential AMPK phosphorylation sites in the presence of AMP. The amount of ^{32}P incorporated into each of the p27 proteins was detected by autoradiography and normalized to p27-WT. A graph depicting the relative amount of phosphorylation is shown below. **(C)** NIH3T3 cells were transfected with plasmids encoding Flag-p27-WT, Flag-p27-S83A, Flag-p27-T197A, Flag-p27-T170A, or Flag-p27-T170D and then analyzed by immunocytochemistry using an anti-Flag antibody. The percentage of cells with either nuclear staining (black bars) or cytoplasmic staining (white bars) was determined by immunocytochemistry using an anti-Flag antibody. Statistical analysis (Fischer test) showed a significant change in localization when comparing either T170A or T170D mutants to WT (a, $p = 0.0147$ and 0.0067, respectively) and when comparing T170A to T170D (b, $p < 0.0001$). **(D)** NIH3T3 cells were transiently transfected with Flag-p27-WT, Flag-p27-S83A, Flag-p27-T170A or Flag-p27-T197A plasmids in combination with the HACA-AMPK-α1 plasmid. Cells were then analyzed by immunocytochemistry using anti-Flag and anti-HA antibodies, and the percentage of cells with CA-AMPK-α1 in which Flag-p27 was detected in the nucleus was quantified. Statistical analysis (Fischer test) showed a significant difference between cells transfected with Flag-p27-T170A and Flag-p27-WT when expressed along with CA-AMPK-α1 (a, $p < 0.0001$). Representative images of immunocytochemistry using anti-HA (CA-AMPK-α1) and anti-Flag antibodies (Flag-p27) are also shown to the right.

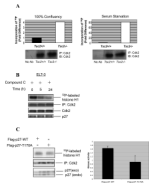

Figure 5.

Elevated Cdk2 activity in tuberin-null cells is suppressed by inhibition of AMPK signaling. **(A)** Whole-cell lysates from *Tsc2*$^{+/+}$ and *Tsc2*$^{-/-}$ MEFs grown to 100% confluency (*left*) or in the absence of serum (*right*) were used for immunoprecipitation of Cdk2. *In vitro* kinase assays were then performed with Cdk2 immunoprecipitates using Histone-H1B as a substrate, and incorporation of ^{32}P into Histone-H1B was detected by autoradiography and quantified (bar graphs). Immunoprecipitates were also analyzed by immunoblotting using an anti-Cdk2 antibody to ensure that equal amounts of Cdk2 were used in kinase assays (*below*). **(B)** ELT-3 cells were treated with 20-μM Compound C for the indicated times and used to generate whole-cell lysates. Lysates were analyzed by immunoblotting using anti-p27 and anti-Cdk2 antibodies or used for immunoprecipitation of Cdk2. Immunoprecipitates were used for *in vitro* kinase assays utilizing Histone-H1B as a substrate or analyzed by immunoblotting using an anti-CDK2 antibody to ensure that equal amounts of Cdk2 were used in kinase assays. Incorporation of ^{32}P into Histone-H1B was detected by autoradiography (*top*). **(C)** ELT-3 cells were transiently transfected with Flag-p27-WT and Flag-p27-T170A. Whole cell lysates were analyzed by immunoblotting using anti-p27 antibody or used for immunoprecipitation of Cdk2. Immunoprecipitates were used for *in vitro* kinase assays utilizing Histone-H1B as a substrate or analyzed by immunoblotting using an anti-Cdk2 antibody. Incorporation of ^{32}P into Histone-H1B was detected by autoradiography and the kinase activity from two independent experiments was measured by densitometric analysis. Statistical analysis (*t*-test) showed a significant decrease in the kinase activity of cells overexpressing Flag-p27-T170A (p=0.05).

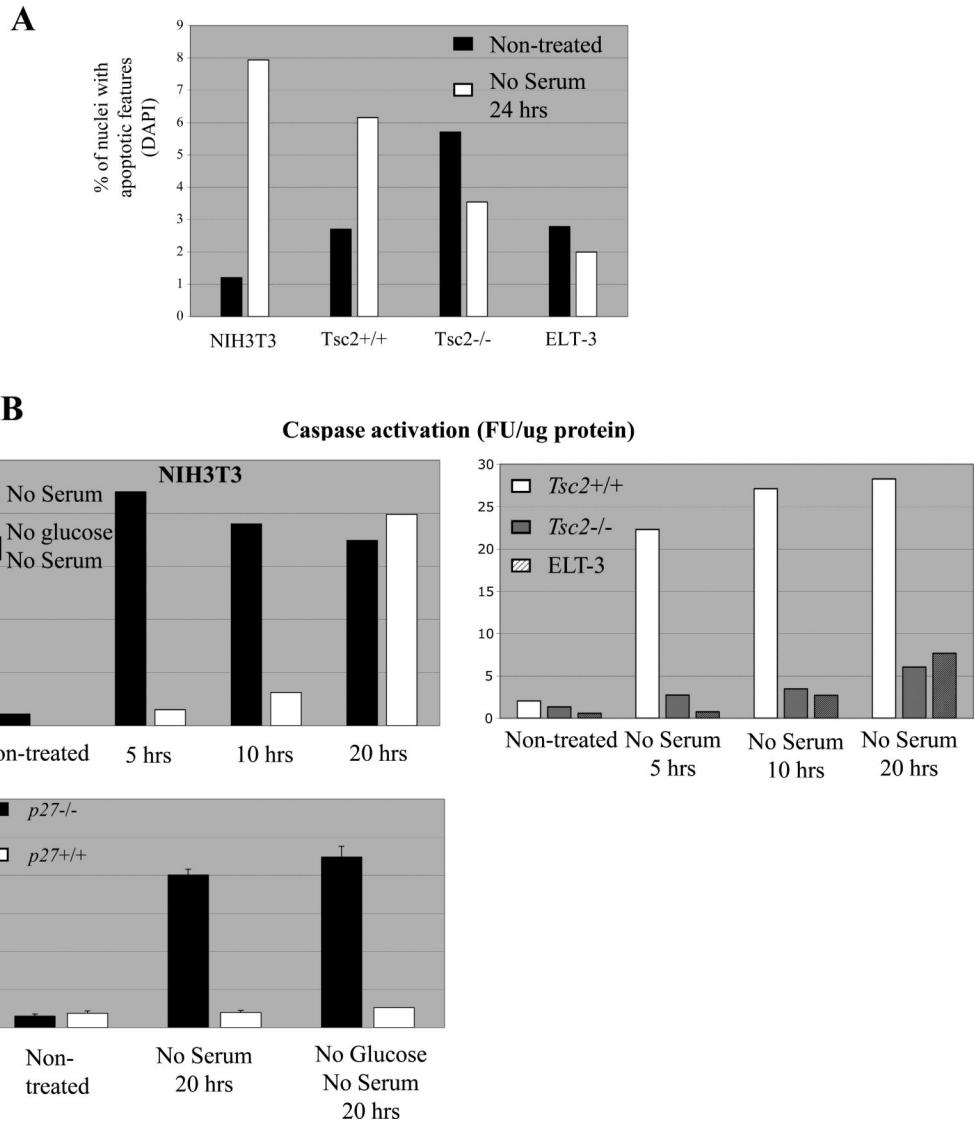

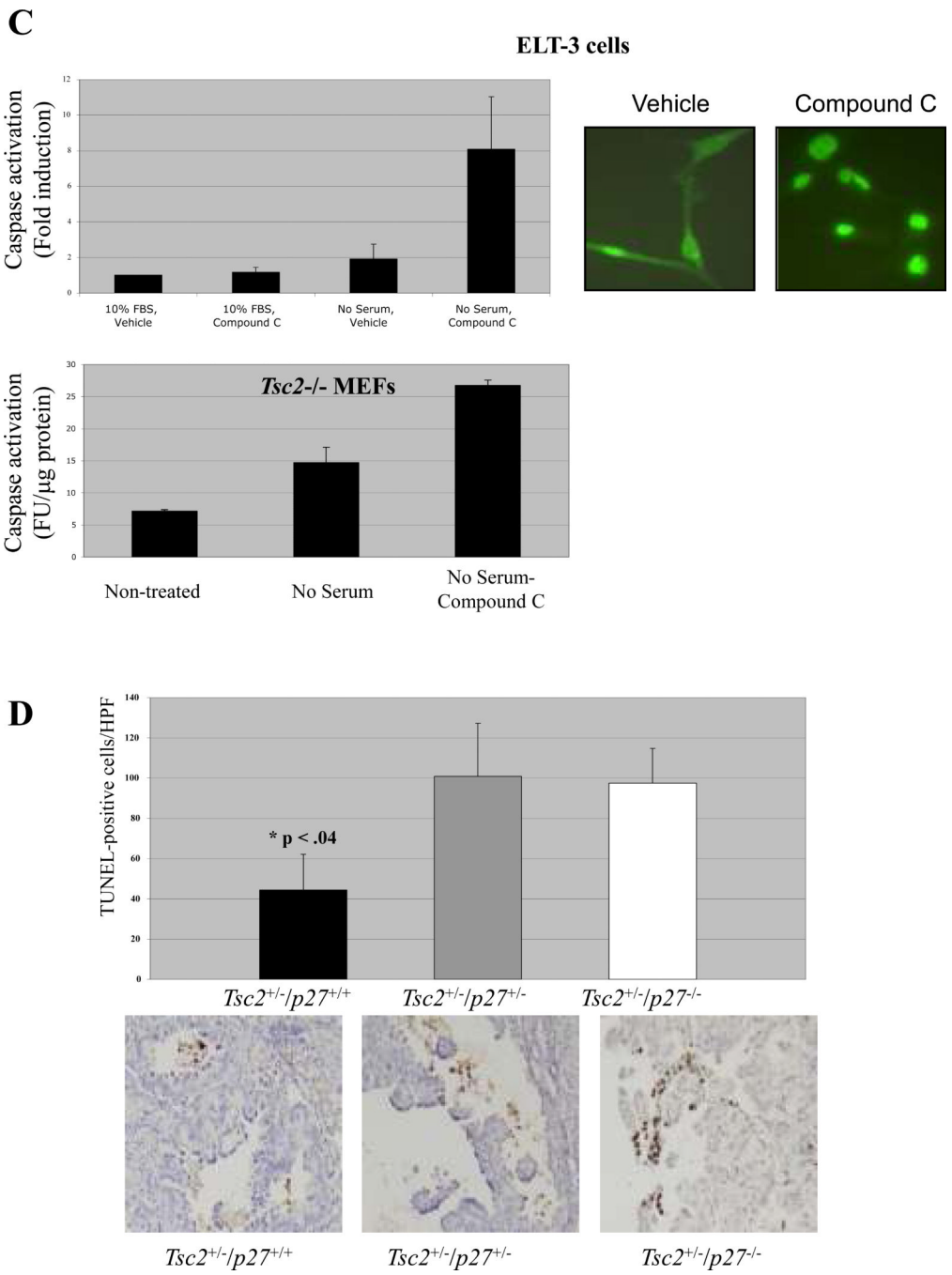

Figure 6.

AMPK activation and cytoplasmic p27 promotes resistance to apoptosis. **(A)** Tuberin-expressing cells (NIH3T3 and $Tsc2^{+/+}$ MEFs) and tuberin-null cells (ELT-3 and $Tsc2^{-/-}$ MEFs) were grown in the presence or absence of serum for 24 hours. Cells were then fixed and stained with DAPI, and the percentage of nuclei with apoptotic features was quantitated via epifluorescent microscopy. **(B)** (*top left*) NIH3T3 cells were deprived of serum in the presence of glucose (black bars) or the absence of glucose (white bars) for the indicated times, and then used to generate whole-cell lysates. (*top right*) $Tsc2^{+/+}$, $Tsc2^{-/-}$ and ELT-3 cells were grown in the absence of serum for the indicated times, and then used to generate whole-cell lysates. (*bottom left*) $p27^{-/-}$ MEF cells and $p27^{+/+}$ MEF cells were deprived of

serum in the presence or absence of glucose for 20 hours, and then used to generate whole-cell lysates. All lysates were then incubated with Ac-DEVD-AFC substrate to determine Caspase-3/Caspase-7 activity, which was measured as fluorescent units of AFC cleaved/μg of protein (FU/μg protein). A representative experiment is shown for each cell line analyzed. **(C)** (*top*) ELT-3 cells were grown in the presence or absence of serum for 5 hours in the absence or presence 20-μM Compound C. Cells were then used to generate whole-cell lysates or analyzed by immunocytochemistry using an anti-p27 antibody (*top right*). Lysates were incubated with Ac-DEVD-AFC substrate to quantitate caspase activity. Caspase activity was normalized to lysates from cells grown in serum without Compound C treatment, and the fold induction of Caspase activity was graphed (*top left*). Three independent experiments were performed, and statistical analysis (Student's t-test) showed a significant increase in caspase activation when comparing serum-starved cells treated with Compound C to vehicle-treated serum-starved cells ($p = 0.022$). (*bottom*) Whole-cell lysates were generated after $Tsc2^{-/-}$ cells had been grown in serum-free media in the absence or presence 20-μM Compound C for 20 hours. Lysates were then incubated with Ac-DEVD-AFC substrate to determine caspase activity, which was measured as fluorescent units of AFC cleaved/μg of protein (FU/μg protein). The mean Caspase activity of Lysates from three independent experiments was quantified. **(D)** Tissue sections from kidney tumors of animals with the indicated genotypes were stained using TUNEL, and TUNEL-positive cells in tumors were quantitated in a blinded fashion to determine number of apoptotic cells/high power field. Statistical analysis (Student's t-test) showed a significant difference in the number of apoptotic cells in $Tsc2^{+/-}/p27^{+/+}$ mice when compared to $Tsc2^{+/-}/p27^{-/-}$ mice ($p = 0.036$). Photomicrographs of representative tumors (20X original magnification) from mice with the indicated genotypes are shown below, and apoptotic cells can be seen with dark brown staining.